INORGANIC CHEMISTRY
FRONTIERS

RESEARCH ARTICLE

View Article Online
View Journal | View Issue

Cite this: *Inorg. Chem. Front.*, 2018, **5**, 619

Crystal structures, phase transitions and thermal expansion properties of $NaZr_2(PO_4)_3$–$SrZr_4(PO_4)_6$ solid solutions†

Ying Liu,[a] Maxim S. Molokeev,[b,c,d] Quanlin Liu[a] and Zhiguo Xia*[a]

Received 10th December 2017,
Accepted 10th January 2018

DOI: 10.1039/c7qi00782e

rsc.li/frontiers-inorganic

Crystal structure evolution and temperature-dependent phase transition of solid solutions are much desired for the understanding of the optimization of functional properties. Herein, the NASICON-type $NaZr_2(PO_4)_3$–$SrZr_4(PO_4)_6$ solid solutions with the formula $Na_{(2-2x)}Sr_x[\,]_xZr_4(PO_4)_6$ ($0 \le x \le 1$), where [ ] represents the vacancy, were prepared by the sol–gel method, and their crystal structures, phase transitions and thermal expansion properties were investigated in detail. In the range of x = 0.3–0.35, there is a reversible structural phase transition $R\bar{3}c \leftrightarrow R\bar{3}$ and the different structural models of the $R\bar{3}$ phase and $R\bar{3}c$ phase were built to better understand the phase transition mechanism. We determined the phase transition boundary between the $R\bar{3}c$ and $R\bar{3}$ structures and predicted the phase transition temperature of $Na_{(2-2x)}Sr_x[\,]_xZr_4(PO_4)_6$ with any x for further investigation of controlled physical properties. The results indicated that $Na_{0.5}Sr_{0.75}[\,]_{0.75}Zr_4(PO_4)_6$ showed a near zero thermal expansion in the temperature range of 450–600 K, which can find potential applications.

1 Introduction

Remarkable progress in different fields of science and technology is boosting the discovery of new solid state materials with optimized functional properties.[1–3] And investigations based on the crystal structure and temperature-dependent phase transition of new solid solutions are very important for the studies of physical properties, such as photoluminescence properties,[4–8] electrical properties[9–13] and thermal expansion,[14–19] especially for inorganic solid state compounds with an open-framework structure. The NASICON structure is among those and consists of a rigid three-dimensional framework of $(PO_4)/(SiO_4)$ tetrahedra sharing common corners with MO_6 octahedra and containing interstitial ions, including alkali and alkaline earth metal ions, located in a three-dimensionally linked interstitial space.[20] As for the NASICON structures, the fast Li-ion conductor lithium zirconium phosphate $LiZr_2(PO_4)_3$ has been studied for fast-ionic conductivity. For example, Al doped $LiZr_2(PO_4)_3$ has been reported for the stability of the highly conducting rhombohedral phase, a decrease in the intensity of impurity phase and an increase in the Li-ion concentration with Al doping, which finally results in a high total Li-ion conductivity;[21] sodium scandium phosphate $Na_3Sc_2(PO_4)_3$ has been reported for the pronounced luminescence property. For example, Im's group reported an $Na_{3-2x}Sc_2(PO_4)_3{:}xEu^{2+}$ phosphor that showed blue emission and did not exhibit thermal quenching even up to 200 °C.[22] $NaZr_2(PO_4)_3$ family compounds have been studied to evaluate the thermal expansion and, for example, it has been reported that $Pb_{2/3}FeZr(PO_4)_{7/3}(SO_4)_{2/3}$ possessed a low thermal expansion with the average linear coefficient of thermal expansion $\alpha_{av} = 1.7 \times 10^{-6}$ °C^{-1} in the temperature range from −120 to 200 °C.[23]

Among the NASICON-type solid state compounds, $NaZr_2(PO_4)_3$ and $SrZr_4(PO_4)_6$, both of which belong to the $NaZr_2(PO_4)_3$ (NZP) family, crystallize in rhombohedral structures but with space groups $R\bar{3}c$ and $R\bar{3}$, respectively. The NZP family ceramics have drawn considerable attention due to their interesting properties, including anisotropic thermal expansion,[24–26] high ionic conductivity,[27,28] and being hosts for the immobilization of nuclear waste.[29,30] From a previous

[a]*The Beijing Municipal Key Laboratory of New Energy Materials and Technologies, School of Materials Sciences and Engineering, University of Science and Technology Beijing, Beijing 100083, China. E-mail: xiazg@ustb.edu.cn; Fax: +86-10-82377955; Tel: +86-10-82377955*
[b]*Laboratory of Crystal Physics, Kirensky Institute of Physics, Federal Research Center KSC SB RAS, Krasnoyarsk 660036, Russia*
[c]*Siberian Federal University, Krasnoyarsk, 660041, Russia*
[d]*Department of Physics, Far Eastern State Transport University, Khabarovsk, 680021, Russia*

†Electronic supplementary information (ESI) available: The crystallographic information files (CIF) of $Na_{(2-2x)}Sr_x[\,]_xZr_4(PO_4)_6$ (x = 0, 0.25, 0.3, 0.35, 0.5, 0.75, and 1), and the high temperature (50–800 °C) dependent XRD patterns and the composition dependent Rietveld refinements of some mentioned samples, coordinates of atoms and main bond lengths of some mentioned compounds. See DOI: 10.1039/c7qi00782e

report, the interstitial ions in the structure play an important role in the thermal expansion of the NZP family ceramics: larger ionic radii or fewer interstitial ions result in lower thermal expansion and some solid solutions in the NZP family are expected to be candidates for structural materials.[31] Although several groups have investigated the thermal properties and crystallographic structures of a wide variety of the NZP family ceramics from room temperature (RT) to 1000 °C,[32–35] studies have seldom been focused on structural phase transformations of the NZP family of solid solutions which is closely related to negative thermal expansion.[36]

In this investigation, we designed and synthesized the nominal $Na_{(2-2x)}Sr_x[\ ]_xZr_4(PO_4)_6$ (x = 0, 0.25, 0.3, 0.35, 0.5, 0.75, and 1) solid solutions, where [ ] represents the vacancy, by the sol–gel method and the samples were mainly characterized by *in situ* variable temperature powder X-ray diffraction (VT-XRD). The structures, phase transitions and thermal expansion were explored in detail. In the present work, the phase transition boundary between the $R\bar{3}c$ and $R\bar{3}$ structures in the $NaZr_2(PO_4)_3$–$SrZr_4(PO_4)_6$ solid solutions has been identified for intermediate x, which can help one to further explore controlled physical properties in the NASICON-type compound family.

2 Experimental section

2.1 Materials and synthesis

A series of $Na_{(2-2x)}Sr_x[\ ]_xZr_4(PO_4)_6$ (x = 0, 0.25, 0.3, 0.35, 0.5, 0.75, and 1) compounds were prepared by the sol–gel method[37–39] from $NaNO_3$ (A. R., Aladdin), $ZrOCl_2{\cdot}8H_2O$ (A. R., Aladdin), $NH_4H_2PO_4$ (A. R., Aladdin), and $Sr(NO_3)_2$ (A.R., Aladdin). Briefly, $NaNO_3$, $Sr(NO_3)_2$, and $ZrOCl_2{\cdot}8H_2O$ were dissolved in distilled water, and, then, the $NH_4H_2PO_4$ aqueous solution was slowly added to the first solution with continuous stirring. At room temperature, the resulting mixture was in the viscous slurry form which was heated at 80 °C for 1 h for gelation. The resulting gel was dried at 150 °C for 4 h, ground, calcined at 700 °C for 6 h, and then finally sintered at 1100 °C for 5 h in a tube furnace. After cooling the furnace to room temperature, the samples were ground into fine powders for subsequent characterization.

2.2 Characterization

The samples of $Na_{(2-2x)}Sr_x[\ ]_xZr_4(PO_4)_6$ with different compositions were characterized using a D8 Advance X-ray diffractometer (XRD, Bruker Corporation, Germany) operating at 40 kV and 40 mA with monochromatized CuKα radiation (λ = 1.5406 Å). The scanning rate (2θ range of 10° to 60°) for phase identification was fixed at 8° min^{-1} and the step size of 2θ was 0.013° and the counting time was 5 s per step for Rietveld analysis. Crystal structure solving and Rietveld refinements were performed using TOPAS 4.2 software.[40] The energy-dispersive X-ray spectroscopy (EDS) and mapping measurements of the selected sample $NaSr_{0.5}[\ ]_{0.5}Zr_4(PO_4)_6$ were performed at room temperature using a scanning electron microscope (SEM, JEOL JSM-6510). Additional X-ray diffraction (XRD) patterns were recorded for $Na_{0.5}Sr_{0.75}[\ ]_{0.75}Zr_4(PO_4)_6$ and $NaSr_{0.5}[\ ]_{0.5}Zr_4(PO_4)_6$ powder samples under heating in the range of 298–1073 K in order to obtain cell parameters dependent on temperature and find the phase transition temperature and thermal expansion properties. The *in situ* variable temperature powder X-ray diffraction (VT-XRD) data were collected on an X'Pert MRD diffractometer with a high-temperature reactor chamber (AntonPaar XRK 900) attached.

3 Results and discussion

3.1 Composition dependent phase transition analysis

Fig. 1a presents the XRD patterns of $Na_{(2-2x)}Sr_x[\ ]_xZr_4(PO_4)_6$ (x = 0, 0.25, 0.3, 0.35, 0.5, 0.75, and 1) solid solutions. Furthermore, the XRD patterns were analyzed by Rietveld refinement with difference Rietveld plots (ESI Fig. S1†), and the refined crystallographic information files are provided in the ESI.† All refinements are stable and give low R-factors (Table 1 and Fig. S2†). The coordinates of atoms and main bond lengths are given in Tables 1S and 2S,† respectively. The main parameters of processing and refinement results are presented in Table 1, and the crystallographic information files (CIF) of these samples are given in the ESI.† The results indicate that compounds with x = 0 and x = 1 are well indexed by

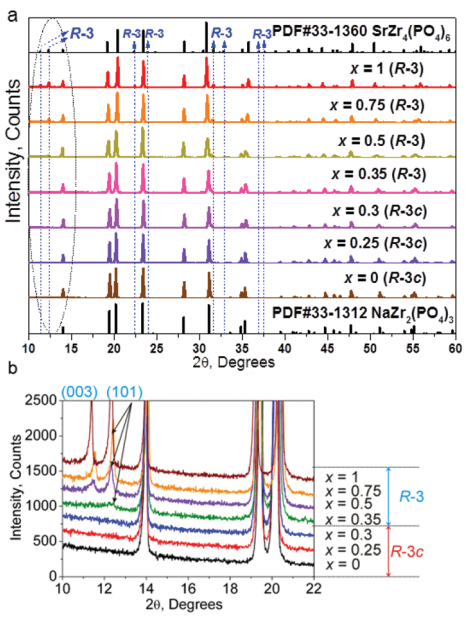

Fig. 1 (a) Powder XRD patterns of various members of the solid solution $Na_{(2-2x)}Sr_x[\ ]_xZr_4(PO_4)_6$ (x = 0, 0.25, 0.3, 0.35, 0.5, 0.75, and 1). With an increase in x, the $R\bar{3}$ phase appears gradually which is marked by the blue dashed arrows. (b) The selected diffraction peaks from 10° to 22° of powder patterns of $Na_{(2-2x)}Sr_x[\ ]_xZr_4(PO_4)_6$ (x = 0, 0.25, 0.3, 0.35, 0.5, 0.75, and 1) which are marked by a black oval in (a). The appearance of structural peaks (0 0 3) and (1 0 1) at x = 0.35 reveals the phase transition boundary $R\bar{3}c \leftrightarrow R\bar{3}$ (also written as $R\bar{3}c \leftrightarrow R\bar{3}$ hereafter and in the figure) between x = 0.3 and x = 0.35.

Table 1 Main parameters of processing and refinement of the $Na_{(2-2x)}Sr_x[\,]_xZr_4(PO_4)_6$ sample

x	$x_{refined}$	Chemical formula	Sp. gr.	Cell parameters	Z	R_{wp}, R_p (%), χ^2	R_B, %
0	0	$NaZr_2(PO_4)_3$	$R\bar{3}c$	a = 8.80898 (7) Å c = 22.7706 (2) Å V = 1530.23 (3) Å^3	2	9.17 6.73 1.55	1.96
0.25	0.13(2)	$Na_{1.5}Sr_{0.25}[\,]_{0.25}Zr_4(PO_4)_6$	$R\bar{3}c$	a = 8.8035 (1) Å c = 22.8502 (3) Å V = 1533.66 (5) Å^3	2	9.87 7.11 1.67	2.11
0.3	0.15(2)	$Na_{1.4}Sr_{0.3}[\,]_{0.3}Zr_4(PO_4)_6$	$R\bar{3}c$	a = 8.7949 (2) Å c = 22.9068 (6) Å V = 1534.47 (8) Å^3	2	11.12 8.11 1.88	2.37
0.35	0.14(1)	$Na_{1.3}Sr_{0.35}[\,]_{0.35}Zr_4(PO_4)_6$	$R\bar{3}$	a = 8.7926 (2) Å c = 22.9186 (5) Å V = 1534.47 (7) Å^3	2	10.52 7.85 1.78	2.67
0.5	0.30(1)	$NaSr_{0.5}[\,]_{0.5}Zr_4(PO_4)_6$	$R\bar{3}$	a = 8.7714 (3) Å c = 23.058 (1) Å V = 1536.3 (1) Å^3	2	12.84 9.77 2.18	3.88
0.75	0.645(8)	$Na_{0.5}Sr_{0.75}[\,]_{0.75}Zr_4(PO_4)_6$	$R\bar{3}$	a = 8.7417 (2) Å c = 23.2083 (5) Å V = 1535.91 (6) Å^3	2	9.83 7.51 1.60	2.49
1	1	$SrZr_4(PO_4)_6$	$R\bar{3}$	a = 8.70925 (5) Å c = 23.3371 (2) Å V = 1532.99 (2) Å^3	2	7.94 5.89 1.35	2.18

rhombohedral unit cells with parameters close to those of $NaZr_2(PO_4)_3$ ($R\bar{3}c$)[41] and $SrZr_4(PO_4)_6$ ($R\bar{3}$),[42] respectively. Therefore, there should be a phase transition boundary $R\bar{3}c \leftrightarrow R\bar{3}$ anywhere in the range of x = 0–1. In the pattern of the sample with x = 1 ($R\bar{3}$), two strong peaks (0 0 3) and (1 0 1) are found (the marked region in Fig. 1a and b), which should be absent in the phase x = 0 ($R\bar{3}c$) due to the extinction rule: (h 0 l), l = 2n + 1. By careful checking of the appearance of these peaks, we can suggest the existence of the phase transition $R\bar{3}c \leftrightarrow R\bar{3}$ in the narrow range of x = 0.3–0.35 (Fig. 1b). Therefore, the crystal structure of $NaZr_2(PO_4)_3$ ($R\bar{3}c$) was taken as the starting model for the Rietveld refinement of the patterns recorded for x = 0, 0.25 and 0.3, while the crystal structure of $SrZr_4(PO_4)_6$ ($R\bar{3}$) was taken for the Rietveld refinement of the patterns obtained for x = 0.35, 0.5, 0.75 and 1. However, some difficulties arose with the structural models of x = 0.35, 0.5, and 0.75. In the $SrZr_4(PO_4)_6$ structure, there is only one Sr site which can be occupied by Sr/Na, but, in this case, the chemical formula can be written as $Na_{(1-x)}Sr_xZr_4(PO_4)_6$ which does not satisfy the charge balancing and is inconsistent with the composition $Na_{(2-2x)}Sr_x[\,]_xZr_4(PO_4)_6$ due to a lack of Na ions. Hence, the crystal structure of the $R\bar{3}$ phase should have an additional site occupied by (1 − x) Na ions. The morphology of the selected sample $NaSr_{0.5}[\,]_{0.5}Zr_4(PO_4)_6$ was studied by SEM analysis (Fig. 2a); relatively uniform crystalline particles were found. Also, the EDS elemental mapping technique was used to test the composition uniformity in $Na_{(2-2x)}Sr_x[\,]_xZr_4(PO_4)_6$ (x = 0.5), as shown in Fig. 2b–f. It is evident that Na, O, P, Sr and Zr are homogeneously distributed over the as-obtained particles.

To further elucidate the crystal structure and composition dependent phase transition, the Fourier difference map $F_{obs} - F_{calc}$ which represents a difference electron density for the Rietveld refinement of structure with x = 0.75 (Fig. 3) was depicted. The map indicates a noticeable maximum at (0 0 1/2) and other symmetry-related sites. It should be noted that

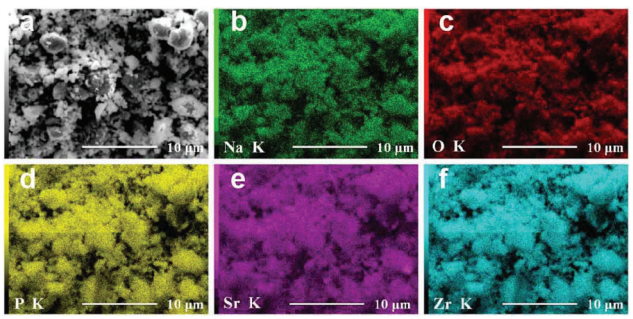

Fig. 2 SEM image (a) of $Na_{(2-2x)}Sr_x[\,]_xZr_4(PO_4)_6$ (x = 0.5) along with EDS elemental mapping for different elements, Na (b), O (c), P (d), Sr (e) and Zr (f).

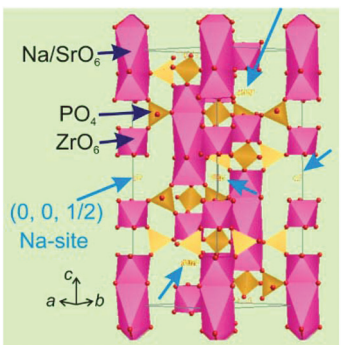

Fig. 3 Fourier difference map of $Na_{(2-2x)}Sr_x[\,]_xZr_4(PO_4)_6$ (x = 0.35) with a maximum at (0 0 1/2) and some other symmetry related points which are marked by blue arrows. All these sites in the $R\bar{3}$ phase should be occupied by (1 − x) Na^+ ions and (x) vacancy.

namely this site is also occupied by Na^+ ions in $NaZr_2(PO_4)_3$ ($R\bar{3}c$); however, the $SrZr_4(PO_4)_6$ ($R\bar{3}$) compound has no Sr^{2+} ions in this site. Therefore, to provide linear evolution from

$Na_{(1-x)}Sr_xZr_4(PO_4)_6$ (x = 0.35) to $SrZr_4(PO_4)_6$ (x = 1), it was decided to refine only $(1-x)$ Na in this site for all compounds with x = 0.35, 0.5, and 0.75. Moreover, the (0 0 0) and (1/2 0 0) sites should differ in the $R\bar{3}$ phase and, as it seems, they should not be occupied by Sr/Na simultaneously. So, finally, the structure of the $R\bar{3}$ phase has two sites: (1) (0 0 0) occupied by $(1-x)$ Na and (x) Sr and (2) (0 0 1/2) occupied by $(1-x)$ Na and (x) vacancy. The structural model of the $R\bar{3}c$ phase has only one site Sr/Na which was occupied by $(1-x)$ Na, (x/2) Sr and (x/2) vacancy.

Based on the refinement results, the dependences of cell parameters of $Na_{(2-2x)}Sr_x[\ ]_xZr_4(PO_4)_6$ on x (Sr^{2+} concentration) are shown in Fig. 4, which reveals two interesting features. Firstly, the cell parameter a (Fig. 4a) and c (Fig. 4b) have a fracture at $x \sim 0.33$, which is in good agreement with the phase transition $R\bar{3}c \leftrightarrow R\bar{3}$ previously found in the narrow range of x = 0.3–0.35 using the analysis of (0 0 3) and (1 0 1) reflection intensities. Secondly, with an increase in the Sr^{2+} concentration (x), the cell parameter a decreases (Fig. 4a), while c increases (Fig. 4b). Such a behavior leads to the nonlinear cell volume (V) dependence on the Sr^{2+} concentration (x) (Fig. 4c) and, even in the range of x = 0.7–1, V decreases with an increase in x despite the fact that the ion radius of Sr^{2+} (CN = 6, 1.18 Å) is larger than that of Na^+ (CN = 6, 1.02 Å). Therefore, we can speculate the existence of a negative thermal expansion (NTE) effect in the compounds $Na_{(2-2x)}Sr_x[\ ]_xZr_4(PO_4)_6$ at x = 0.7–1. It should be noted that the refined values of x are slightly smaller than the expected ones (Table 1 and Fig. 4d); so the real concentration interval of such NTE compounds can be 0.5–1 instead of 0.7–1. Anyway, the expected and refined values of Sr concentrations are comparable and the overall increase trend in the Sr^{2+} concentration is consistent (Fig. 4d).

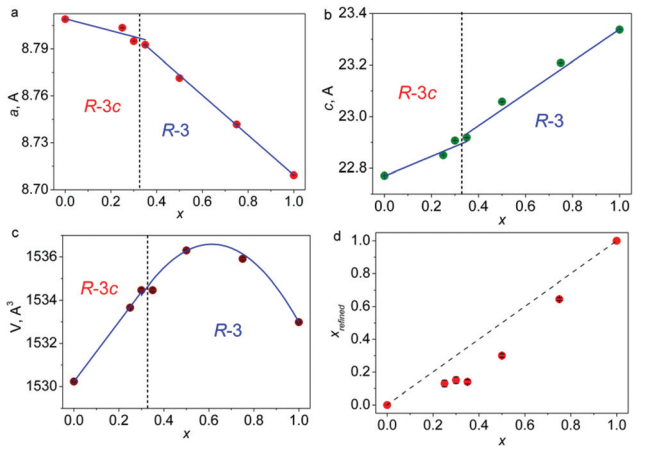

Fig. 4 Dependences of cell parameters (a) a, (b) c and (c) cell volume V per x. (d) Dependence of the refined value $x_{refined}$ of the Sr concentration in the compounds $Na_{(2-2x)}Sr_x[\ ]_xZr_4(PO_4)_6$ per suggested concentration x. Ideally, all points should lie in the straight line which is depicted by the dashed line in Fig. 4(d). In our case, there is some deviation from the suggested chemical formula, but the overall trend of the Sr concentration increase is the same.

Theory group investigation of the phase transition $R\bar{3}c \leftrightarrow R\bar{3}$ using the ISODISTORT program[43] revealed that the transformation can be described by the emergence of instability at the (0 0 0) k7-point (Γ) of the Brillouin zone of the high-symmetry $R\bar{3}c$ unit cell (hereinafter the designation of irreducible representations (irrep) and points of the Brillouin zone are given in accordance with reference books).[44,45] The Γ_2^{+} irrep drives this phase transition, and the transformation can be written as $R\bar{3}c \overset{\Gamma_2^{+}(\eta)}{\longleftrightarrow} R\bar{3}$, where η is the critical order parameter. The analysis presents that this irrep allows a continuous phase transition and, indeed, there is no jump of cell volume or cell parameters when the phase transition occurs (Fig. 4a–c). It should be noted that the phase transition leads to charge ordering and splitting of positions. For example, the Na site in the $R\bar{3}c$ structure splits into two sites for the $R\bar{3}$ phase: Na1 at the (0 0 0) site and Na2 at the (0 0 1/2) site. Namely, these two sites were suggested during building the structural model of $Na_{(2-2x)}Sr_x[\ ]_xZr_4(PO_4)_6$ in the $R\bar{3}$ phase though the pure $SrZr_4(PO_4)_6$ ($R\bar{3}$) has only one filled site (0 0 0) and one vacancy site (0 0 1/2).

Taking into account all obtained information, we can build a model of structural transformation for $NaZr_2(PO_4)_3$ doped with Sr^{2+} ions (Fig. 5). The compound $NaZr_2(PO_4)_3$ crystallizes in the $R\bar{3}c$ group with only one Na site in the asymmetric part of the unit cell. Low Sr^{2+} concentration in the range of x = 0–0.3 doesn't lead to space group changing and only the ionic

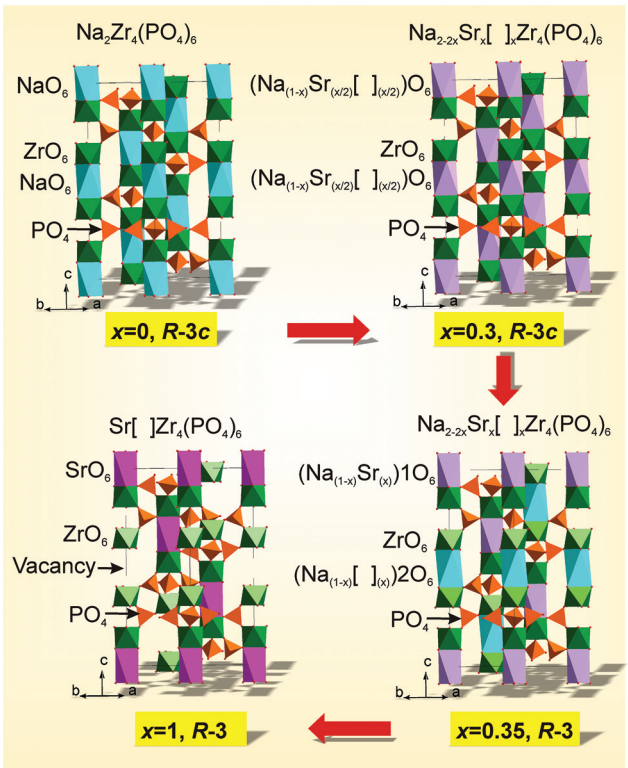

Fig. 5 Crystal structure modification from $Na_2Zr_4(PO_4)_6$ to $SrZr_4(PO_4)_6$ through $Na_{(2-x)}Sr_x[\ ]_x(PO_4)_6$. Phase transition $R\bar{3}c \leftrightarrow R\bar{3}$ with charge ordering and splitting of positions happens in the range of x = 0.3–0.35.

replacement ($2Na^+ \leftrightarrow Sr^{2+}$ + vacancy) happens. The higher Sr^{2+} concentration level leads to the phase transition and the Na site splits into two cation sites. The Na1 site is occupied by $(1 - x)$ Na and (x) Sr ions, while the Na2 site is occupied by $(1 - x)$ Na and, so, again the replacement scheme ($2Na^+ \leftrightarrow Sr^{2+}$ + vacancy) is valid. The vacancy part in the Na2 site increases with an increase in x up to total disappearance of any ion in this site at $x = 1$ (Fig. 5).

3.2 Temperature dependent phase transition and thermal expansion property

In order to prove the existence of NTE in these compounds, the temperature dependent XRD patterns of two representative powder samples, $NaSr_{0.5}[\ ]_{0.5}Zr_4(PO_4)_6$ (Fig. S1†) and $Na_{0.5}Sr_{0.75}[\ ]_{0.75}Zr_4(PO_4)_6$ (Fig. S2†), were measured and they are given in the ESI.† Some interesting facts were revealed in this investigation. First of all, the measurements made for the sample $x = 0.5$ clearly show that the cell parameter a decreases under heating (Fig. 6a), with the coefficients of thermal expansion (CTE) -3.0×10^{-5} K^{-1} ($R\bar{3}$) and -2.1×10^{-5} K^{-1} ($R\bar{3}c$) (298–1073 K), which proves the linear negative thermal expansion in this crystallographic direction. Comparatively, the sample $x = 0.75$ shows the cell parameter a decreasing in (NTE) the range of 300–450 K, near zero thermal expansion (ZTE) in the range of 450–600 K and, at higher temperatures, the cell parameter a increasing with the coefficient of thermal expansion varied from -6.4×10^{-6} to 3.1×10^{-6} K^{-1} (298–1073 K) (Fig. 7a). Such behavior is extremely unusual and near zero thermal expansion is a very useful property because ceramics of this composition will be less strained under heating/cooling which leads to a good mechanical feature. It should be noted that the point $x = 0.75$ is in close vicinity to the point corresponding to the maximum of the $V(x)$ curve (Fig. 4c). Thus, one can suppose that the Sr^{2+} concentration (x) at which the compounds have such an unusual property can be located near this maximum, *i.e.* $x = 0.6$–0.8.

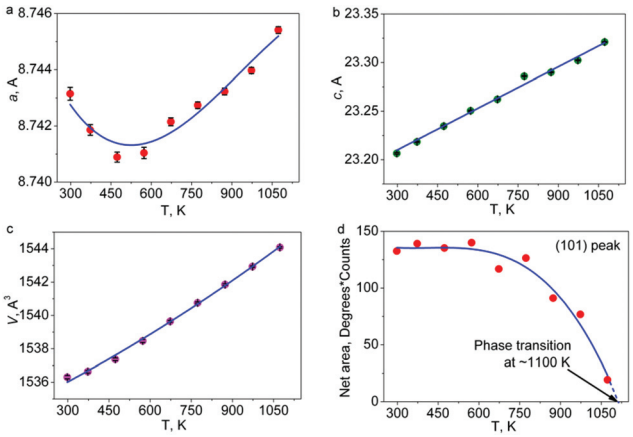

Fig. 7 Temperature dependences of (a) cell parameter a; (b) cell parameter c; (c) cell volume V and (d) net area of the superstructure peak (101) of $Na_{(2-2x)}Sr_x[\ ]_xZr_4(PO_4)_6$, $x = 0.75$.

Secondly, it can be seen that $NaSr_{0.5}[\ ]_{0.5}Zr_4(PO_4)_6$ has a phase transition $R\bar{3}c \leftrightarrow R\bar{3}$ upon heating at $T \sim 700$ K, because the intensity of the superstructure peak (101) becomes zero (Fig. 6d) and all cell parameters and the cell volume possess jumps at this temperature (Fig. 6a–c). Thus this transition cannot be of the second order type. The $Na_{0.5}Sr_{0.75}[\ ]_{0.75}Zr_4(PO_4)_6$ sample has no phase transition in the temperature region of 25–800 °C (Fig. 7a–d), but the extrapolation presents that the intensity of the superstructure peak (101) should become zero at ~1100 K (Fig. 7d). It should be noted that the sample $Na_{(2-2x)}Sr_x[\ ]_xZr_4(PO_4)_6$ ($x \sim 0.32$) should have such a phase transition at room temperature $T \sim 300$ K (Table 1 and Fig. 4a–c), and all the three points ($x = 0.32$, $T = 300$ K), ($x = 0.5$, $T = 700$ K), and ($x = 0.75$, $T = 1100$ K) lie on one straight line (Fig. 8). This line is the phase transition boundary between $R\bar{3}c$ and $R\bar{3}$ and it can provide us the means for prediction of the phase transition temperature in $Na_{(2-2x)}Sr_x[\ ]_xZr_4(PO_4)_6$ with other x.

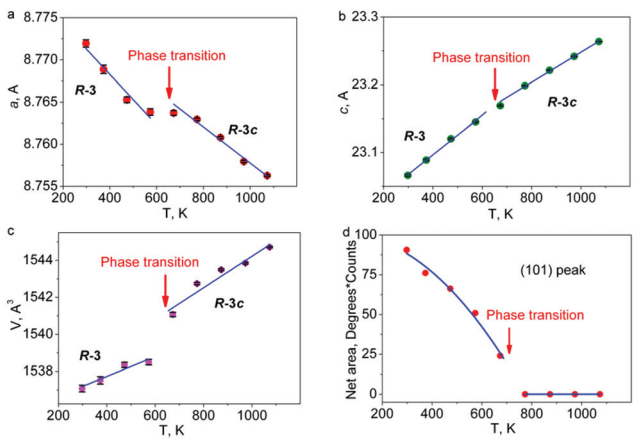

Fig. 6 Temperature dependences of (a) cell parameter a; (b) cell parameter c; (c) cell volume V and (d) net area of the superstructure peak (101) of $Na_{(2-2x)}Sr_x[\ ]_xZr_4(PO_4)_6$, $x = 0.5$.

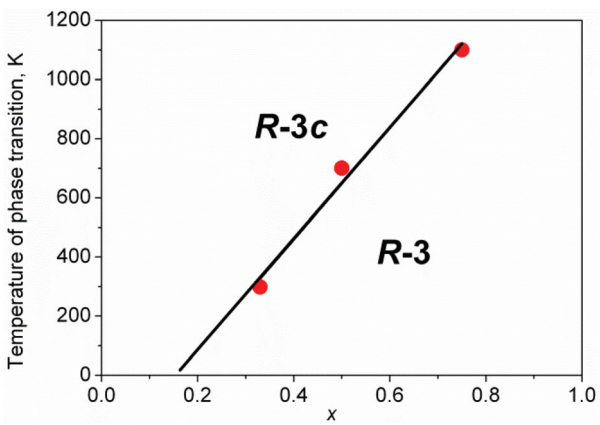

Fig. 8 Linear increase of the phase transition temperature with an increase in Sr concentration x.

4 Conclusion

In summary, we have designed and synthesized the NASICON-type $Na_{(2-2x)}Sr_x[\ ]_xZr_4(PO_4)_6$ ($0 \le x \le 1$) solid solutions by the sol–gel method and studied the crystal structures, thermal expansion properties and phase transitions of samples using XRD techniques. Notably, the ZTE property is achieved in $Na_{(2-2x)}Sr_x[\ ]_xZr_4(PO_4)_6$ (x = 0.75) in the temperature range of 450–600 K. In the range of x = 0.3–0.35, there is a structural phase transition $R\bar{3}c \leftrightarrow R\bar{3}$. The structure of the $R\bar{3}$ phase has two sites: (0 0 0) occupied by $(1-x)$ Na and (x) Sr and (0 0 1/2) occupied by $(1-x)$ Na and (x) vacancy, while the structural model of the $R\bar{3}c$ phase has only one site Sr/Na which was occupied by $(1-x)$ Na, $(x/2)$ Sr and $(x/2)$ vacancy. In the temperature range of 298–1073 K, the CTE of $NaSr_{0.5}[\ ]_{0.5}Zr_4(PO_4)_6$ was -3.0×10^{-5} K^{-1} ($R\bar{3}$) and -2.1×10^{-5} K^{-1} ($R\bar{3}c$), while $Na_{0.5}Sr_{0.75}[\ ]_{0.75}Zr_4(PO_4)_6$ exhibited a near zero thermal expansion in the range of 450–600 K and the CTE ranges from -6.4×10^{-6} to 3.1×10^{-6} K^{-1} (298–1073 K) which suggests their potential application as specific structural materials. Finally, we determined the phase transition between the $R\bar{3}c$ and $R\bar{3}$ structures and predicted the phase transition temperature of $Na_{(2-2x)}Sr_x[\ ]_xZr_4(PO_4)_6$ at arbitrary x.

Conflicts of interest

There are no conflicts to declare.

Acknowledgements

The present work was supported by the National Natural Science Foundation of China (Grants 91622125, 51722202 and 51572023) and the Natural Science Foundations of Beijing (2172036), and M. Molokeev acknowledges support of the Russian Foundation for Basic Research (17-52-53031).

Notes and references

1 H. Wu, H. Yu, Z. Yang, X. Hou, X. Su, S. Pan, K. Poeppelmeier and J. Rondinelli, *J. Am. Chem. Soc.*, 2013, **135**, 4215–4218.
2 G. Li, K. Wu, Q. Liu, Z. Yang and S. Pan, *J. Am. Chem. Soc.*, 2016, **138**, 7422–7428.
3 X. Wang, Y. Wang, B. Zhang, F. Zhang, Z. Yang and S. Pan, *Angew. Chem., Int. Ed.*, 2017, **56**, 14119–14123.
4 Z. Xia, G. Liu, J. Wen, Z. Mei, M. Balasubramanian, M. S. Molokeev, L. Peng, L. Gu, D. J. Miller, Q. Liu and K. R. Poeppelmeier, *J. Am. Chem. Soc.*, 2016, **138**, 1158–1161.
5 M. Zhao, Z. Xia, M. S. Molokeev, L. Ning and Q. Liu, *Chem. Mater.*, 2017, **29**, 6552–6559.
6 H. Nakagawa, S. W. Kim, T. Hasegawa, S. Hasegawa, T. Ishigaki, K. Uematsu, K. Toda, H. Takabad and M. Sato, *Inorg. Chem. Front.*, 2017, **4**, 1562–1567.
7 M. Chen, Z. Xia, M. S. Molokeev, T. Wang and Q. Liu, *Chem. Mater.*, 2017, **29**, 1430–1438.
8 H. Ji, Z. Huang, Z. Xia, M. S. Molokeev, V. V. Atuchin and S. Huang, *Inorg. Chem.*, 2014, **53**, 11119–11124.
9 M. Samanta and K. Biswas, *J. Am. Chem. Soc.*, 2017, **139**, 9382–9391.
10 S. Kumar and P. Balaya, *Solid State Ionics*, 2016, **296**, 1–6.
11 V. Diez-Gomez, K. Arbi and J. Sanz, *J. Am. Chem. Soc.*, 2016, **138**, 9479–9486.
12 Q. Ma, M. Guin, S. Naqash, C.-L. Tsai, F. Tietz and O. Guillon, *Chem. Mater.*, 2016, **28**, 4821–4828.
13 A. M. Abakumov, M. D. Rossell, O. Y. Gutnikova, O. A. Drozhzhin, L. S. Leonova, Y. A. Dobrovolsky, S. Y. Istomin, G. V. Tendeloo and E. V. Antipov, *Chem. Mater.*, 2008, **20**, 4457–4467.
14 Z. Pan, J. Chen, L. Fan, H. Liu, L. Zhang, L. Hu, Y. Ren, L. Liu, L. Fang, X. Fan, Y. Li and X. Xing, *Inorg. Chem. Front.*, 2017, **4**, 1352–1355.
15 S. E. Tallentire, F. Child, I. Fall, L. Vella-Zarb, I. R. Evans, M. G. Tucker, D. A. Keen, C. Wilson and J. S. Evans, *J. Am. Chem. Soc.*, 2013, **135**, 12849–12856.
16 C. R. Morelock, L. C. Gallington and A. P. Wilkinson, *Chem. Mater.*, 2014, **26**, 1936–1940.
17 C. Thieme, T. Waurischk, S. Heitmann and C. Russel, *Inorg. Chem.*, 2016, **55**, 4476–4484.
18 W. Cao, Q. Li, K. Lin, Z. Liu, J. Deng, J. Chen and X. Xing, *RSC Adv.*, 2016, **6**, 96275–96280.
19 F. Han, L. Hu, Z. Liu, Q. Li, T. Wang, Y. Ren, J. Deng, J. Chen and X. Xing, *Inorg. Chem. Front.*, 2017, **4**, 343–347.
20 N. Anantharamulu, K. Koteswara Rao, G. Rambabu, B. Vijaya Kumar, V. Radha and M. Vithal, *J. Mater. Sci.*, 2011, **46**, 2821–2837.
21 Y. Zhang, K. Chen, Y. Shen, Y. Lin and C. W. Nan, *Ceram. Int.*, 2017, **43**, 598–602.
22 Y. H. Kim, P. Arunkumar, B. Y. Kim, S. Unithrattil, E. Kim, S. H. Moon, J. Y. Hyun, K. H. Kim, D. Lee, J. S. Lee and W. B. Im, *Nat. Mater.*, 2017, **16**, 543–550.
23 V. I. Pet'kov, A. S. Dmitrienko, M. V. Sukhanov, A. M. Koval'skii and E. Y. Borovikova, *Russ. J. Inorg. Chem.*, 2016, **61**, 623–629.
24 T. Oota and I. Yamai, *J. Am. Chem. Soc.*, 1986, **69**, 1–6.
25 D. A. Woodcock and P. Lightfoot, *J. Mater. Chem.*, 1999, **9**, 2907–2911.
26 V. I. Pet'kov, A. I. Orlova, G. N. Kazantsev, S. G. Samoilov and M. L. Spiridonova, *J. Therm. Anal. Calorim.*, 2001, **66**, 623–632.
27 A. K. Ivanov-Schitz and A. B. Bykov, *Solid State Ionics*, 1997, **100**, 153–155.
28 W. Wang, B. Jiang, L. Hu and S. Jiao, *J. Mater. Chem. A*, 2014, **2**, 1341–1345.
29 V. I. Pet'kov, A. I. Orlova, I. G. Trubach, Y. A. Asabina and V. W. Demarin, *Czech J. Phys.*, 2003, **53**, 640–648.
30 R. Raja Madhavan, A. S. Gandhi and K. V. Govindan Kutty, *Ceram. Interfaces*, 2017, **43**, 9522–9530.

31 H. Miyazaki, I. Ushiroda, D. Itomura, T. Hirashita, N. Adachi and T. Ota, *Jpn. J. Appl. Phys.*, 2008, **47**, 7262–7265.
32 T. Ota, P. Jin and I. Yamai, *J. Mater. Sci.*, 1989, **24**, 4239–4245.
33 I. Yamai and T. Ota, *J. Am. Chem. Soc.*, 1992, **75**, 2276–2282.
34 K. V. Govindan Kutty, R. Asuvathraman and R. Sridharan, *J. Mater. Sci.*, 1998, **33**, 4007–4013.
35 G. Buvaneswari, K. V. Govindan Kutty and U. V. Varadaraju, *Mater. Res. Bull.*, 2004, **39**, 475–488.
36 P. P. Sahoo, S. Sumithra, G. Madras and T. N. Row, *Inorg. Chem.*, 2011, **50**, 8774–8781.
37 D. K. Agrawal and J. H. Adair, *J. Am. Ceram. Soc.*, 1990, **73**, 2153–2155.
38 K. Kamali, T. R. Ravindran, C. Ravi, Y. Sorb, N. Subramanian and A. K. Arora, *Phys. Rev. B: Condens. Matter Mater. Phys.*, 2012, **86**, 144301.
39 K. Kamali, T. R. Ravindran, N. V. Chandra Shekar, K. K. Pandey and S. M. Sharma, *J. Solid State Chem.*, 2015, **221**, 285–290.
40 *Bruker AXS TOPAS V4: General profile and structure analysis software for powder diffraction data-User's Manual*, Bruker AXS, Karlsruhe, Germany, 2008.
41 H. P. Hong, *Mater. Res. Bull.*, 1976, **11**, 173–182.
42 C. Rashmi and O. Shrivastava, *Solid State Sci.*, 2011, **13**, 444–454.
43 B. J. Campbell, H. T. Stokes, D. E. Tanner and D. M. Hatch, *J. Appl. Crystallogr.*, 2006, **39**, 607–614.
44 O. V. Kovalev, *Representations of the Crystallographic Space Groups: Irreducible Representations, Induced Representations, and Corepresentations*, Gordon and Breach Science, 1993.
45 S. C. Miller and W. F. Love, *Tables of irreducible representations of space groups and co-representations of magnetic space groups*, Pruett Press, 1967.